Supporting Information:

Ultra-low Lattice Thermal Conductivity Realizes Ultra-High Performance $Bi_{0.48}Sb_{1.52}Te_3$-Based Thermoelectric Material and Module

Hongtao Li, Lidong Chen, Zhe Guo,* Gang Wu, Xiaojian Tan,* Qiang Zhang, Jianfeng Cai, Qianqian Sun, Jacques G. Noudem, Peng Sun, Jiehua Wu, Guo-Qiang Liu, Jun Jiang*

H. Li

School of Material Science and Chemical Engineering, Ningbo University

Ningbo 315211, China

H. Li, L. Chen, Dr. Z. Guo, G. Wu, Prof. X. Tan, Dr. Q. Zhang, J. Cai, Q. Sun, P. Sun, Prof. J. Wu, Prof. G.-Q. Liu, Prof. J. Jiang

Ningbo Institute of Materials Technology and Engineering, University of Chinese Academy of Sciences

Ningbo 315201, China

E-mail: guozhe@nimte.ac.cn, tanxiaojian@nimte.ac.cn, jjun@nimte.ac.cn

L. Chen, Dr. Z. Guo, G. Wu, Prof. X. Tan, Dr. Q. Zhang, J. Cai, Q. Sun, P. Sun, Prof. G.-Q. Liu, Prof. J. Jiang

University of Chinese Academy of Sciences

Beijing 100049, China

Prof. J. G. Noudem

Normandie University, ENSICAEN, UNICAEN, CNRS, CRISMAT

Caen 14000, France

Materials and methods

Sample Synthesis: To synthesize the $Sn_{1/3}Ge_{1/3}Pb_{1/3}Te$ (SGPT) compound, high-purity (5N) elemental Sn, Ge, Pb, and Te mixture was sealed in an evacuated quartz tube and melted at 800 K for 4 hours and then quenched in cool water for the SGPT single phase ingot. High-purity (5N) elemental Bi, Sb, Cu, Sn, Ge, Pb and Te granules were weighed according to the stoichiometric ratio of $Bi_{0.48}Sb_{1.52}Te_3$ (BST) + x wt% SGPT (x = 0.30, 0.50) and $Bi_{0.48}Sb_{1.516}Cu_{0.004}Te_3$ + 0.50 wt% SGPT (y = 0.002, 0.003, 0.004, 0.005), and the mixtures were sealed into Ø10 mm vacuum quartz tubes. The quartz tubes were heated at 1023 K for 1 hours and then rocked for 1 hours, and finally quenched to room temperature in water. The quenched ingots were then ground into powders using a high-speed vibrational ball mill (MSK-SFM-3, China). Finally, the powders were cast into Ø20 mm graphite dies and spark plasma sintered at 693 K under 60 MPa for 5 min.

Structure Characterization and Measurement: Powder X-ray diffraction (PXRD, Bruker D8, Germany) was used for characterized the phase compositions of each sample after ball milling with a Cu Kα (λ = 1.5406 Å). The microstructures of grains were characterized by electron backscatter diffraction (EBSD) carried out on a scanning electron microscopy (SEM, Quanta FEG 250, FEI). Transmission electron microscopy (TEM, 2100F, Japan) was further applied to analyse the microstructure of the $Bi_{0.48}Sb_{1.516}Cu_{0.004}Te_3$ + 0.50 wt% SGPT sample. The bars were cut and polished into the dimension of 12 × 3 × 3 mm^3 to simultaneously measure the electrical conductivity σ and Seebeck coefficient S using a ZEM-3 apparatus (Ulvac-Riko, Japan). The thin wafers with a size of 10 × 10 × 1 mm^3 were used to determine the thermal diffusion coefficient D through the laser flash diffusivity method (Netzsch LFA467, Germany). Then, the total thermal conductivity κ_{tot} was evaluated by the equation $\kappa_{tot} = D\rho C_p$, where density ρ was determined by Archimedes' method while the specific heat C_p was obtained by the Dulong–Petit law. The room-temperature Hall coefficients R_H of all samples were determined using a physical property measurement system (PPMS-9,

Quantum Design, USA). Then the carrier concentration n_H and mobility μ_H were calculated by the formulas $n_H = 1/(eR_H)$ and $\mu_H = \sigma R_H$, respectively.

TE Module Fabrication and Measurement: The TE module contains 17 pairs of p-n legs with an overall size of 20 mm × 20 mm. The Ni diffusion barrier layer was prepared by thermal spraying. The Pb-Bi and Sn-Bi based solders were used for the hot side and the cold side, respectively. The module performance was evaluated by a home-built test system, and the energy conversion efficiency η was obtained as $\eta = P/(Q_c + P) \times 100\%$, where P was the measured output power and Q_c was the measured cold-side heat flow.

Statistical analysis: The electronic and thermal transport parameters were assessed using the commercial ZEM-3 and LFA-457 instruments, respectively. The observed results exhibit minimal dependency on sample size, with errors primarily stemming from the standard deviations inherent to these instruments. Notably, the systematic errors associated with the Seebeck coefficient S and electrical conductivity σ measurements approximate 3% and 5%, respectively. The composite uncertainty for the total thermal conductivity κ_{tot} is estimated at approximately 7%, wherein the contributions are apportioned as 1% for density ρ, 5% for specific heat C_p, and 5% for thermal diffusion D. Consequently, the uncertainty associated with the zT value is projected to be around 10%. Since the examination of thermal conductivity of Cu has an uncertainty of 5% and the uncertainties of output voltage and current are 0.5%, the uncertainty of conversion efficiency is about 6%, similar to the previous report.[1]

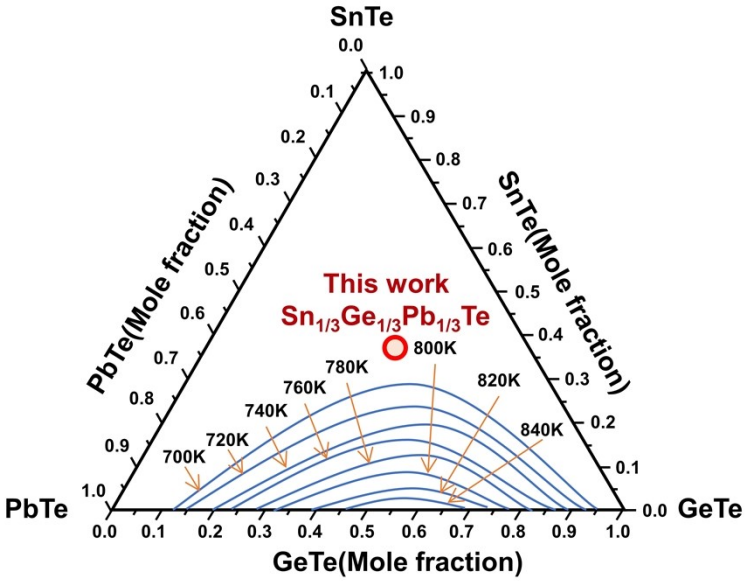

Figure S1. Phase diagrams for SnTe-PbTe-GeTe at various isotherms[2]

Structure model of the $Sn_{1/3}Ge_{1/3}Pb_{1/3}Te$ and $Bi_{0.48}Sb_{1.52}Te_3$

SGPT possesses a cubic crystal structure with a space group of *Pm3m*. Compounds are formed by replacing the vacancies of Ge atoms with Sn or Pb. The corresponding schematic diagrams of composites of SGPT and BST are depicted in Figure S2.

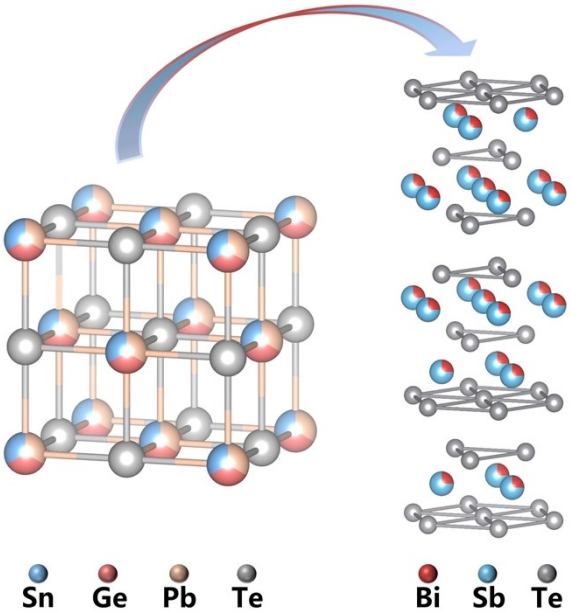

Figure S2. Schematic diagram of the crystal structure of SGPT and BST.

Table S1. The XRD refinement results for lattice parameters of BST and $Bi_{0.48}Sb_{1.516}Cu_{0.004}Te_3$ + 0.50 wt % SGPT representative samples.

Samples		*x*=0.0, *y*=0.0	*x*=0.50, *y*=0.004
Lattice Parameters(Å)	*a/b*	4.29482	4.28885
	c	30.43123	30.47123

At the melting temperature of BST, SGPT exhibits marginal stability, whereby crystal decomposition may prompt the substitution of Cu (1.17 Å), Sn (1.40 Å), Ge (0.53 Å), or Pb (1.19 Å) for Sb (1.41 Å) or Bi (1.46 Å). This substitution leads to a slight reduction in the lattice parameters along the a- and b-axes, while the c-axis experiences a slight increase, possibly due to partial occupancy of copper atoms in van der Waals interlayer positions. The variations in lattice constants suggest successful doping of SGPT and copper into BST, forming a stable solid solution.

Calculated The calculation of orientation factor *F*

The calculation of the orientation factor (*F*), which serves as an indicator of the degree of orientation in layered-structural samples, is conducted using the Lotgering method. It is expressed by the following equation:[3]

$$F = \frac{P - P_0}{1 - P_0}$$

$$P = \frac{\sum I(00l)}{\sum I(hkl)}$$

$$P_0 = \frac{\sum I_0(00l)}{\sum I_0(hkl)}$$

Here, $\Sigma I(00l)$ represents the total intensity of all (*00l*) planes' diffraction peaks, $\Sigma I(hkl)$ represents the total intensity of all (*hkl*) diffraction peaks, and P is the ratio of (*00l*) plane intensity to the total intensity in the measured data. Similarly, ΣI_0 (*00l*), $\Sigma I(hkl)$, and P_0 denote the corresponding parts of the standard powder diffraction file. In the X-ray patterns of incompletely oriented materials, the (*hkl*) reflections persist, and the ratio of the intensity of the (*00l*) and (*hkl*) reflections increases with stronger orientation. The orientation factor ranges from 0 to 1, signifying the extent of orientation, from no preferred orientation to complete orientation.

The calculated orientation factors F_{00l} for a series of samples are tabulated below. Notably, samples fabricated through ball milling and spark plasma sintering methods exhibit markedly low F_{00l} values, ranging from 0.045 to 0.070.

Table S2. Orientation factors F_{00l} for the $Bi_{0.48}Sb_{1.52-y}Cu_yTe_3$ + *x* wt%SGPT samples at room temperature.

x/*y*	F_{00l}
0/0	0.05623
0.30/0	0.06864
0.50/0	0.06969
0.50/0.002	0.05684
0.50/0.003	0.06774
0.50/0.004	0.06993
0.50/0.004	0.06328

TEM characterizations of $Bi_{0.48}Sb_{1.516}Cu_{0.004}Te_3$ + 0.50 wt%SGPT sample

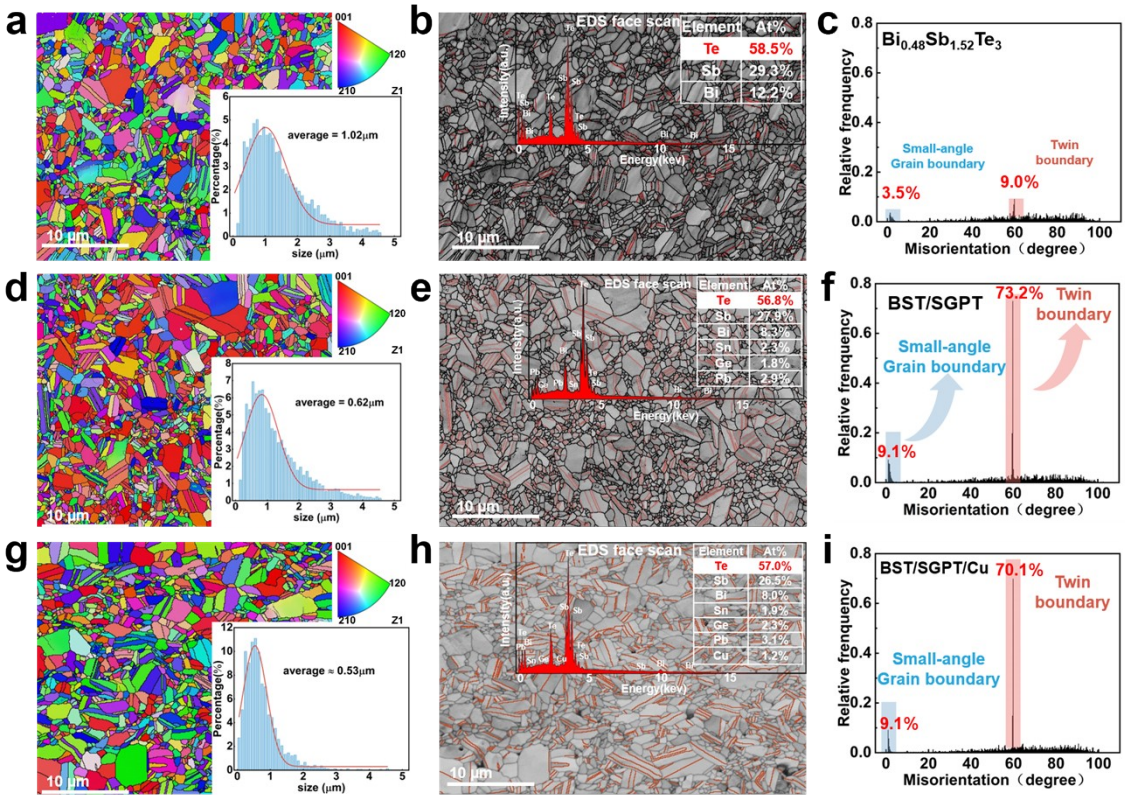

Figure S3. a), d),and g) The inverse pole figure and grain size distributionbe, b), e), and h) Kikuchi band contrast map (the red line indicates the twin boundaries at 60°) and the corresponding EDS elemental mappings (face scan), c), f), and i) grain boundary misorientation distribution for BST, $Bi_{0.48}Sb_{1.52}Te_3$ + 0.50 wt%SGPT and $Bi_{0.48}Sb_{1.516}Cu_{0.004}Te_3$ + 0.50 wt%SGPT samples.

Geometric phase analysis: This method involves aligning the *x* direction with the (110) crystal plane and ensuring that the *y* direction is perpendicular to the (110) crystal plane. In this context, ε_{xx} and ε_{yy} represent the normal strains in the *x* and *y* directions, respectively, while ε_{yy} and Δ_{xy} indicate the shear strains in the *xy* and *yx* directions, respectively.

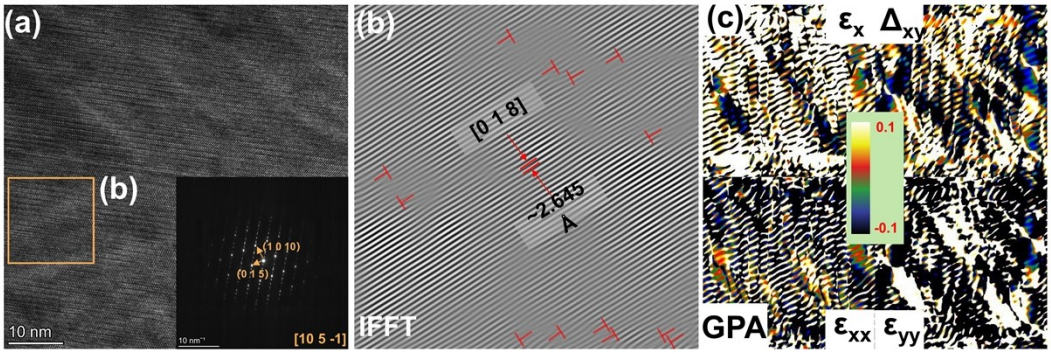

Figure S4. TEM images for the $Bi_{0.48}Sb_{1.516}Cu_{0.004}Te_3$ + 0.50 wt%SGPT sample. (a) High-resolution TEM image of $Bi_{0.48}Sb_{1.516}Cu_{0.004}Te_3$ + 0.50 wt%SGPT matrix and SAED patterns along [10 5 -1] zone axis, (b) IFFT image of "Area b" in (b), and (c) GPA image of the area corresponding to "Area b".

Calculation of κ_{ph} and κ_{bip}

Disregarding the bipolar effect at lower temperatures, the value of $\kappa_{ph} + \kappa_{bip}$ is approximately equal to the value of κ_{ph}. The κph data around 300 K can be fitted with the expression $\kappa_{ph} = aT^{-1} + b$, where a and b are the fitting parameters. Then the fitted κ_{ph} is obtained by extrapolating the equation to 500 K. Finally, the fitted κ_{ph} and calculated κ_e are subtracted from the measured κ_{tot} to obtain the κ_{bip} values for all samples between 300~500 K.

Table S3. Fitting parameters for all the $Bi_{0.48}Sb_{1.52-y}Cu_yTe_3$ + *x* wt%SGPT samples by using the expression of $\kappa_{ph} = aT^{-1} + b$.

x/y	*a*	*b*
0/0	24.45786	0.56952
0.30/0	28.19879	0.50638
0.50/0	33.72441	0.42063
0.50/0.002	67.24948	0.30066
0.50/0.003	81.38919	0.24556
0.50/0.004	75.75550	0.17605
0.50/0.004	99.44537	0.09810

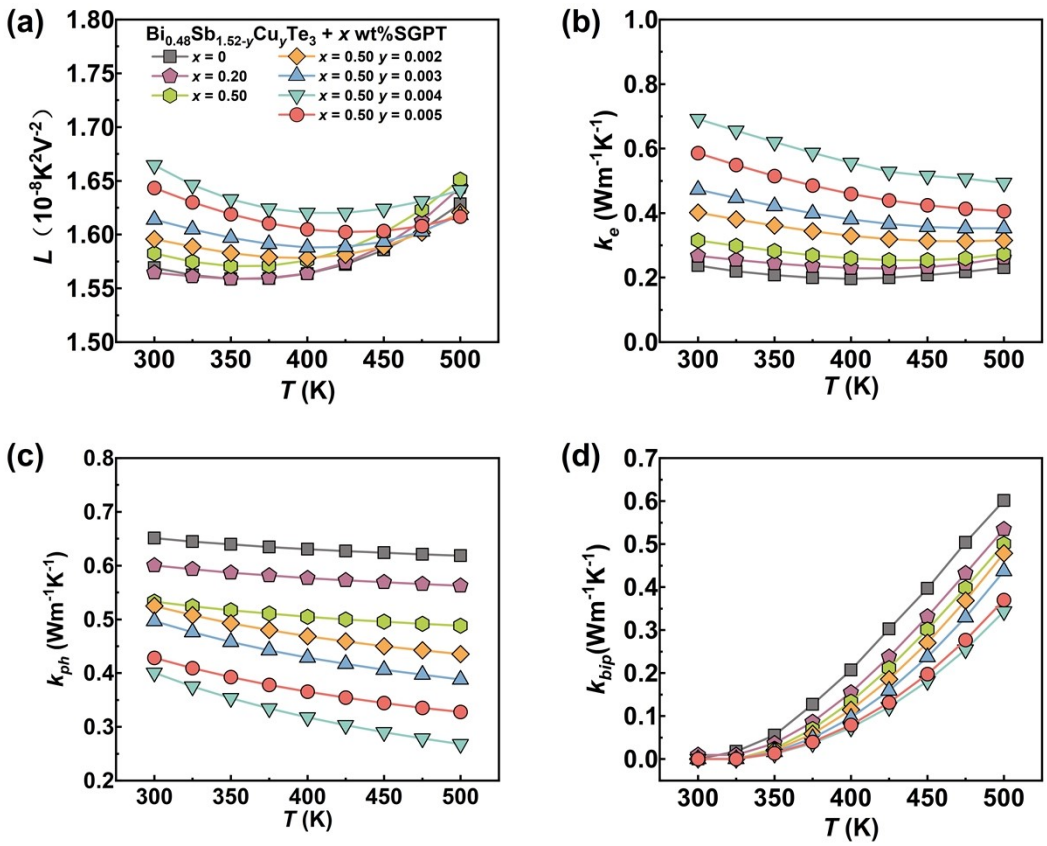

Figure S5. Thermal transport properties for $Bi_{0.48}Sb_{1.52-y}Cu_yTe_3$ + *x* wt%SGPT (*x*=0.30, 0.50, *y*= 0.002, 0.003, 0.004, 0.005) samples: (a) Calculated Lorenz number *L* for $Bi_{0.48}Sb_{1.52-y}Cu_yTe3$ + *x*wt% SGPT, and (b) electronic thermal conductivity κ_e, (c) lattice thermal conductivity κ_{ph}, and (d) bipolar thermal conductivity κ_{bip}.

Single parabolic band model

The electronic transport properties of thermoelectric semiconductors can be well simulated by the single parabolic band model. The Seebeck coefficient can be described as:[4,5]

$$S = \frac{k_B}{e}\left[\frac{(r+5/2)F_{(r+3/2)}(\eta)}{(r+3/2)F_{(r+1/2)}(\eta)} - \eta\right] \quad \text{(S2)}$$

where the scattering factor r is –1/2 when the charge carriers are mainly scattered by acoustic phonons; η is the reduced Fermi energy $\eta = \frac{E_f}{k_B T}$ and $F_i(\eta) = \int_0^\infty \frac{x^i}{1+e^{x-\eta}} dx$ is the *ith* order Fermi integral. By fitting the experimental results of Seebeck coefficient versus carrier concentration n, the corresponding reduced Fermi energy η is obtained, and then the density of state effective mass can be evaluated as:

$$m_d^* = \frac{h^2}{2k_B T}\left[\frac{nr_H}{4\pi F_{1/2}(\eta)}\right]^{2/3} \quad \text{(S3)}$$

Then, the Hall carrier concentration and Hall factor are expressed as:

$$n = \frac{1}{eR_H} = \frac{8\pi(2m_d^* k_B T)^{3/2}}{3h^3} \frac{(r+3/2)^2 F_{(r+1/2)}^2(\eta)}{(2r+3/2)F_{(2r+1/2)}(\eta)} \quad \text{(S4)}$$

$$r_H = \frac{3(2r+3/2)F_{1/2}(\eta)F_{(2r+1/2)}(\eta)}{2(r+3/2)^2 F_{(r+1/2)}^2(\eta)} \quad \text{(S5)}$$

Moreover, the deformation potential parameter is determined by:

$$E_{def}^2 = \frac{\sqrt{2}\pi(h/2\pi)^4 e\rho v_L^2}{3(m_d^*)^{5/2}(k_B T)^{3/2} F_{1/2}(\eta)\mu_H} r_H \quad \text{(S6)}$$

where C_l is the elastic constant for longitudinal vibrations, ρ is density, and v_L is the longitudinal velocity of sound. Based on the above equations, the Hall mobility is evaluated as:

$$\mu_H = \left[\frac{e\pi h^4 C_1}{\sqrt{2}(k_B T)^{3/2} E_{def}^2 (m^*)^{5/2}}\right] \frac{(2r+3/2)F_{(2r+1/2)}(\eta)}{(r+3/2)^2 F_{(r+1/2)}(\eta)} \quad \text{(S7)}$$

Debye-Callaway model

According to the Debye-Callaway model, the lattice thermal conductivity with doping or alloying can be calculated with the following equation,

$$\kappa_{ph} = \frac{k_B}{2\pi^2 v}\left(\frac{k_B T}{\hbar}\right)^3 \int_0^{\theta_D/T} \tau_{tot}(x)\frac{x^4 e^x}{(e^x-1)^2}dx$$

The integrand item in conjunction with the coefficient of Eq.(S7) is the spectral lattice thermal conductivity (κ_s), namely,

$$\kappa_s = \frac{k_B}{2\pi^2 v}\left(\frac{k_B T}{\hbar}\right)^3 \tau_{tot}(x)\frac{x^4 e^x}{(e^x-1)^2}$$

where $x = \hbar\omega/k_B T$ (ω denoting the phonon frequency) is the reduced phonon frequency, $\hbar$ is the reduced Plank constant, k_B is the Boltzmann constant, v is average sound speed, ϑ_D is the Debye temperature. τ_{tot} is the total relaxation time and can be evaluated via the Matthiessen's rule. Here, we mainly consider phonon-phonon Umklapp scattering (U), grain boundary scattering (B), point defect scattering (PD), nano-precipitates scattering (NP), and stacking faults scattering (SF),

$$\tau_{tot}^{-1} = \tau_U^{-1} + \tau_B^{-1} + \tau_{PD}^{-1} + \tau_{NP}^{-1} + \tau_{SF}^{-1}$$

The Umklapp phonon-phonon scattering (U),

$$\tau_U^{-1} = A_N \frac{2}{(6\pi^2)^{1/3}} \frac{k_B \bar{V}^{1/3} \gamma^2 \omega^2 T}{\bar{M} v^3}$$

where A_N is the prefactor of Umklapp scattering time, $\bar{V}$ is the average atomic volume, γ is the Grüneisen parameter, $\bar{M}$ is the average atomic mass.

The grain boundary phonon scattering (B),

$$\tau_B^{-1} = \frac{v}{d}$$

where d is the average grain size.

The point defect phonon scattering (PD),

$$\tau_{PD}^{-1} = \frac{k_B^4 \bar{V}}{4\pi\hbar^4 v^3}\Gamma x^4 T^4 \quad \text{and} \quad \Gamma = \sum_i f_i\left(\frac{\bar{m}-m_i}{\bar{m}}\right)^2$$

where Γ is the point defect scattering parameter and determined by the mass difference.

The nano precipitates phonon scattering (NP),

$$\tau_{NP}^{-1} = v\left[\left(2\pi R^2\right)^{-1} + \left(\frac{4}{9}\pi R^2(\Delta D/D)^2(\omega R/v)^4\right)^{-1}\right]^{-1} N_p$$

where R is the average radius for the precipitates, ΔD is density difference between the precipitate and matrix, D is the matrix density, N_p is the number density of precipitates.

The stacking faults phonon scattering (SF),

$$\tau_{SF}^{-1} = 0.7\frac{a^2}{v}\gamma^2\omega^2 N_s$$

where a is the lattice parameter, and N_s is the number of stacking faults crossing a line of unit length. The parameters required for the Debye-Callaway model are summarized in Table S4.

Table S4. Parameters for calculating κ_{ph} of the $Bi_{0.48}Sb_{1.516}Cu_{0.004}Te_3$+0.50 wt%SGPT sample in the Debye-Callaway model.

Parameters	Descriptions	Values	Ref
v	In-plane average speed of sound	2147 m s^{-1}	6
ϑ_D	Debye temperature	94K	7
V	Average atomic volume	31.26 $Å^3$	6
γ	Grüneisen parameter	2.33	8
B_D	Effective Burger's vecto	1.2×10^{-19} m	fitted
v_L	Longitudinal sound velocity	2884 m s^{-1}	9
v_T	Transverse sound velocity	1780 m s^{-1}	7
V_{BT}	Atomic volume of Bi_2Te_3	3.40×10^{-29} m^3	10
V_{ST}	Atomic volume of Sb_2Te_3	3.31×10^{-29} m^3	8
M_{BT}	Atomic mass of Bi_2Te_3	2.79×10^{-25} kg	7
M_{ST}	Atomic mass of Sb_2Te_3	2.07×10^{-25} kg	7
C_0	Concentration of $Bi_{0.48}Sb_{1.52}Te_3$ in Bi_2Te_3	0.25	11
K	Bulk modulus	44.8 GPa	7
T_a	Sintering temperature	693 K	Exp.
d	Grain size	2×10^{-6} m	Exp.
r	Poisson's ratio	2.33	12
N_d	Dislocation density	3.33×10^{14} cm^{-2}	Exp.
Γ	Point defect scattering parameter	0.23	Exp.
R	Average radius of second phase	20 nm	Exp.
N_P	Number density of Second phase	7.33×10^{19} m^3	Exp.
D	Density of matrix	6.65 g/cm^3	Exp.

The calculation of average *zT*

Given the inherent temperature dependence of thermoelectric parameters, assessing the thermoelectric properties of materials within a specific temperature range through computation of the average *zT* (zT_{avg}) is imperative. The formula for calculating zT_{avg} is as follows:

$$zT_{avg} = \frac{\int_{T_c}^{T_h} zT\,dT}{T_h - T_c}$$

Where T_h, T_c are the hot-side and cold-side temperatures, respectively.

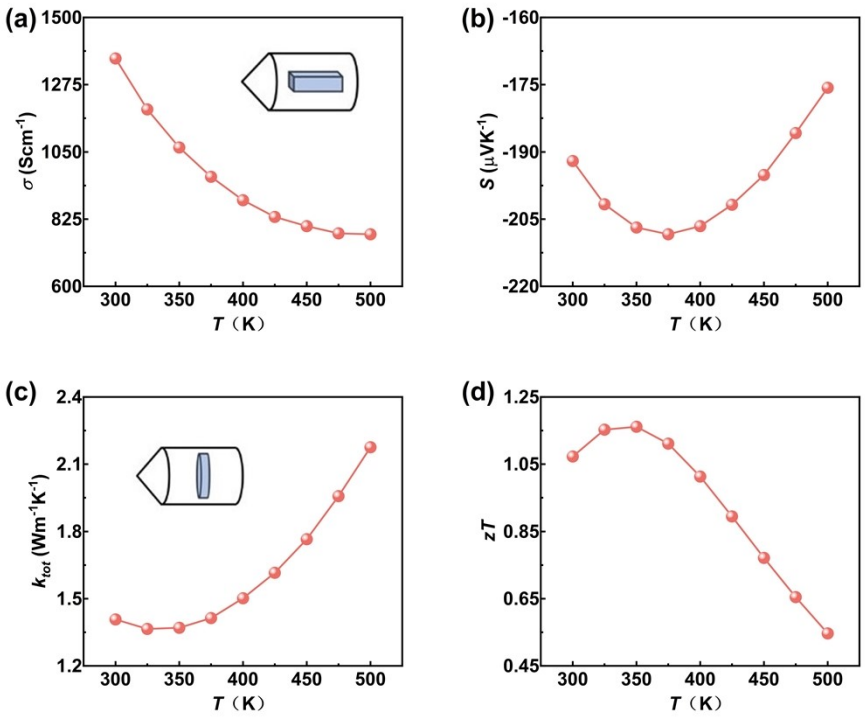

Figure S6. Temperature dependence of (a) electrical conductivity, (b) Seebeck coefficient, (c) total thermal conductivity, and (d) zT value for previously reported zone-melted $Bi_2Te_{2.7}Se_{0.3}$ materials used to assemble the thermoelectric module. The orientation of the test samples in the ingot is shown in figures (a) and (c).

Homemade test system diagram

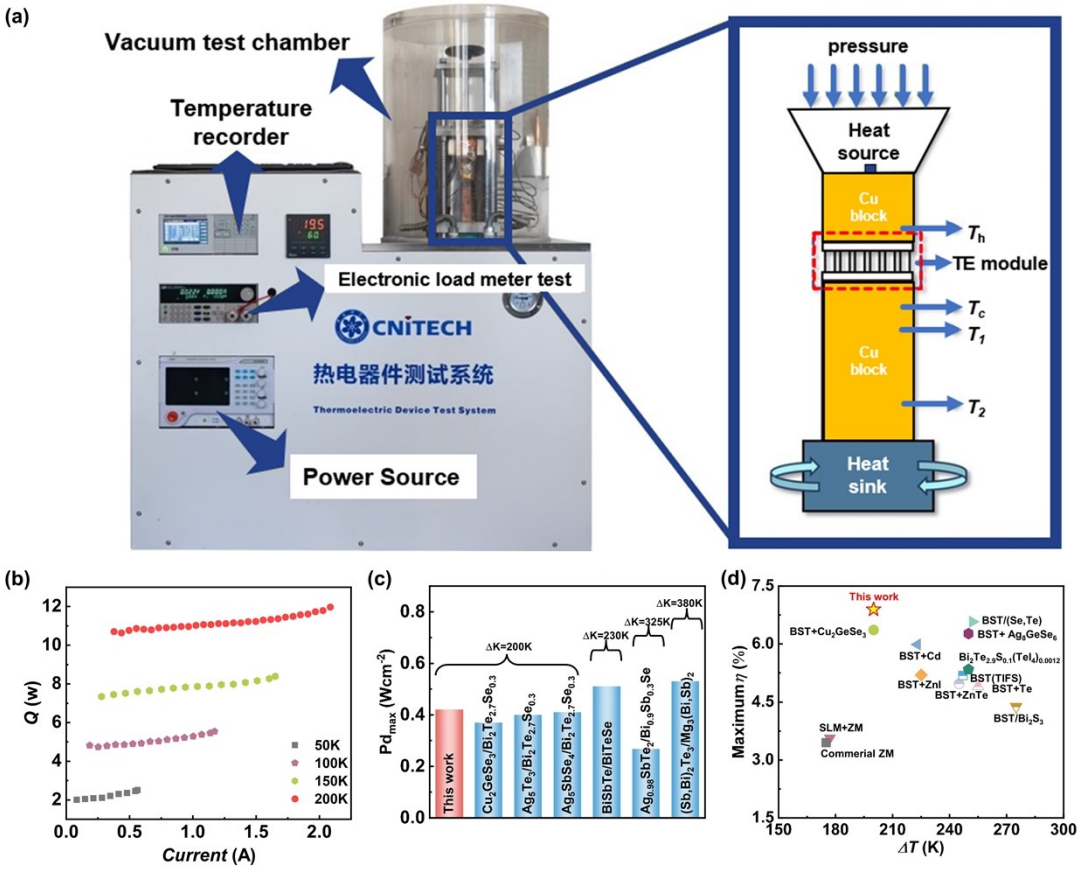

Figure S7. (a) Homemade test system diagram. (b) The measured heat flow *Q* of the fabricated thermoelectric module. (c) The comparison of power density of $Bi_{0.48}Sb_{1.516}Cu_{0.004}Te_3$ + 0.50 wt% SGPT /$Bi_2Te_{2.7}Se_{0.3}$ module, and (d) the maximum conversion efficiency of the fabricated TE module compared with previously reported Bi_2Te_3-based TE modules.

References:

[1] L. Yin, X. Li, X. Bao, J. Cheng, C. Chen, Z. Zhang, X. Liu, F. Cao, J. Mao, Q. Zhang, *Nat. Commun.* 2024, **15**, 1468.

[2] J. Tang, Z. Yao, Y. Wu, S. Lin, F. Xiong, W. Li, Y. Chen, T. Zhu and Y. Pei, *Mater. Today Phys.*, 2020, **15**, 100247.

[3] K. Pang, L. Miao, Q. Zhang, Q. Pan, Y. Liu, H. Shi, J. Li, W. Zhou, Z. Zhang, Y. Zhang, G. Wu, X. Tan, J. G. Noudem, J. Wu, P. Sun, H. Hu, G. Liu and J. Jiang, *Adv. Funct. Mater.*, 2024, 2315591.

[4] J. Zhu, X. Zhang, M. Guo, J. Li, J. Hu, S. Cai, W. Cai, Y. Zhang and J. Sui, *NPJ Comput. Mater.*, 2021, **7**, 116.

[5] J. Shen, X. Zhang, Z. Chen, S. Lin, J. Li, W. Li, S. Li, Y. Chen and Y. Pei, *J. Mater. Chem. A*, 2017, **5**, 5314–5320.

[6] V. A. Kulbashinskii, V. G. Kytin, N. V. Maslov, P. Singha, S. Das, A. K. Deb and A. Banerjee, *Mater. Today: Proc.*, 2019, **8**, 573–581.

[7] K. Pang, M. Yuan, Q. Zhang, Y. Li, Y. Zhang, W. Zhou, G. Wu, X. Tan, J. G. Noudem, C. Cui, H. Hu, J. Wu, P. Sun, G. Liu and J. Jiang, *Small*, 2023, **6**, 2306701.

[8] Q. Zhang, M. Yuan, K. Pang, Y. Zhang, R. Wang, X. Tan, G. Wu, H. Hu, J. Wu, P. Sun, G. Liu and J. Jiang, *Adv. Mater.*, 2023, **35**, 2300338.

[9] P. F. Rosen and B. F. Woodfield, *J. Chem. Thermodyn.*, 2020, **141**, 105974.

[10] E. S. Toberer, A. Zevalkink and G. J. Snyder, *J. Mater. Chem.*, 2011, **21**, 15843–15852.

[11] T. Ikeda, *Materia Japan*, 2014, **53**, 307–311.

[12] X. Chen, H. D. Zhou, A. Kiswandhi, I. Miotkowski, Y. P. Chen, P. A. Sharma, A. L. Lima Sharma, M. A. Hekmaty, D. Smirnov and Z. Jiang, *Appl. Phys. Lett.*, 2011, **99**, 261912.